RSC Advances

ROYAL SOCIETY OF CHEMISTRY

www.rsc.org/advances

Hydroquinone as single precursor for concurrent reduction and growth of carbon nanotubes on graphene oxide

Vadahanambi Sridhar, Inwon Lee, Ho-Hwan Chun and Hyun Park *

Global Core Research Center for Ships and Offshore Plants (GCRC-SOP),

Pusan National University, *Busan 609-735, Republic of Korea*

AUTHOR EMAIL ADDRESS: hyunpark@pusan.ac.kr;

RECEIVED DATE (to be automatically inserted after your manuscript is accepted if required according to the journal that you are submitting your paper to)

TITLE RUNNING HEAD Concurrent reduction and growth of carbon nanotubes on graphene oxide

;

ABSTRACT. Effective reduction and inhibiting restacking are critical steps in realizing the full potential of chemically derived graphene. In this manuscript, we report a one-step, all solid-state microwave procedure for simultaneous reduction and concurrent growth of carbon nanotubes 'spacers' on graphene from a single precursor, namely hydroquinone. Our newly developed technique not only effectively reduces graphene oxide but also results in vertically anchored carbon nanotubes on graphene substrate to give unique mesoporous, hierarchical carbon nano-architectures. When applied as negative electrode in lithium-ion batteries, our 3D graphene-carbon nanotube hybrids exhibit high capacity of 1016 $mAhg^{-1}$ with a columbic efficiency of 98% even after prolonged cycling.

KEYWORDS. Graphene, carbon nanotubes, cobalt, 3D nano architectures, lithium ion battery.

Introduction

The discovery of outstanding properties of graphene synthesized by 'scotch tape method' by Geim and Novoselov,[1] spurred many research efforts to synthesize graphene sheets in a bulk quantity. Several techniques broadly classified as '*top down*' and '*bottom up*' synthesis have been developed. Of these, the '*top down*' synthesis by oxidative treatment of graphite to graphene oxide followed by its subsequent reduction is the most widely researched due to its low-cost and capability of large-scale production of graphene. [2] However there are two critical steps which affects the overall performance of reduced graphene oxide(rGO), the first being effective reduction of graphene oxide to graphene and second, the more critical step is inhibiting the tendency of graphene sheets to restack due to inherent van der Waal's π-π attractions. For reduction of graphene oxide, physical techniques like heating and annealing in inert atmosphere, [3] infra-red, [4] ultraviolet, [5] sunlight, [6] and the more prevalent chemical reducing agents[7-10] have been reported. However, many of these chemical reducing agents are used in liquid form and the obtained rGO quickly restacks itself into multilayer graphene in aqueous solutions. A common way of mitigating the restacking phenomenon is by using surfactants and other capping reagents which reduce inter-sheet attractive forces and keeps chemically reduced graphene in fairly exfoliated state. [11] But most surfactants have polyatomic ions which anchor on the graphene sheets, considerably reducing the conductivity of graphene.[12] Another way of dealing the problem of restacking is by using 'spacers' like polymer chains, [13] zero-dimensional(0-D) metal nano-particles, [14] carbon nano structures like nano-cups, [15] hollow spheres, [16] nano-walls[17] etc. Of these, metal-separated graphene sheets are most widely reported and the graphene-metal composites are highly desirous in energy storage applications like super capacitors, [18] electrode materials in lithium-[19] and sodium -ion batteries, [20] transparent substrates in dye sensitized solar cells, [21] catalysts in oxygen reduction[22] and hydrogen evolution reactions[23] etc. When compared to 0-D metal nanoparticles, using anisotropic one-dimensional(1-D) structures like nano-wires, [24] nano-rods, [25] and nano-tubes[26] are beneficial and impart properties such as large surface area, high porosity and different physical and

electronic properties. An interesting 1-D spacer are carbon nanotubes(CNT), the 1-D rolled up graphenic nano-structures, incorporated in the inter-lamellar space of graphene which not only prevents its restacking and increase the basal spacing, but also improves the volumetric electrical conductivity. [27] Recently there have been efforts to hybridize these two nano-carbon allotropes to obtain three dimensional (3-D) nano-structures and these were found to be perform better as transparent conductors,[28] photocatalysis, [29] lithium-ion batteries, [30] supercapacitors, [31] and fuel cells[32] when compared to their individual constituents.

The synthesis of graphene-CNT (G-CNT) hybrids can be broadly classified as *ex-situ* and *in-situ*. *Ex-situ* techniques involves simple physical mixing of either pristine or oxidized CNT and graphene oxide dispersions[33] and subsequent reduction and self-assembly of these two nano-carbon structures due to the van der Waal's interactions. There are some reports on fabrication of G-CNT hybrids by self-assembly of functionalized graphene and/or CNT, [34] and using layer-by-layer (LbL) assembly.[35] But in all the above reported *ex-situ* techniques, carbon nanotubes are horizontally anchored on the graphene substrate and the perceived advantages of G-CNT hybrids is minimal due to the 'eclipsing' of active surface area of graphene by horizontally aligned CNT whereas common sense dictates that in order to get maximum synergistic effect, the optimized architecture is vertically anchoring carbon nanotubes on graphene substrate. Some '*in-situ*' techniques on synthesis of G-CNT hybrids by chemical vapor deposition (CVD) method using a multi-step process: (i) synthesis of graphene, (ii) grafting of catalyst particles onto the graphene surface and (iii) subsequent growth of CNT on the surface of the catalyst have been reported. [36-39] Though CVD synthesis is an effective way of growing dense CNT forests on graphene substrates, but it suffers from disadvantages like requirement of capital cost intensive specialized equipment, high purity inert gases (argon and/or nitrogen) and explosive hydrocarbon gases(methane or acetylene). An alternative technique is microwave synthesis of CNT which offers advantages such as faster synthesis, low capital costs on equipment and ability to synthesize CNT in normal atmospheric conditions. But till date, only three precursors: ionic liquids, [40] metallocenes[41,42] and polymeric initiators like azo-bis-cyclohexane carbonitrile (AICN) [43] have been used to synthesize

CNT by microwave methods. Therefore, there is a need for alternative precursors for microwave *in-situ* synthesis of G-CNTs.

Herein we report a simple microwave-based technique to synthesize carbon nanotubes vertically anchored on graphene(G-Co@CNT) nano-hybrid structures using hydroquinone (HQ) as the source of carbon nanotubes and cobalt as the catalyst. The utility of aqueous HQ solution as reducing agent for graphene oxide is already reported[44] and our newly developed all-solid state synthesis technique not only effectively reduces graphene oxide but grafts CNT vertically on the graphene substrate to yield high volume synthesis of functionalized three dimensional carbon nano-hybrids. The applicability of synthesized G-Co@CNT as anode materials in lithium ion battery is also investigated.

Experimental

Materials and Methods

Graphene oxide was prepared from high purity expandable graphite (purity of 99%, average size of 200 μm; purchased from Samjung C & G, Korea) using a modified Hummer's method.[8] Reagent grade cobalt acetate and hydroquinone were purchased from Aldrich and were used as received. Microwave irradiation was carried out in a domestic microwave oven manufactured by Daewoo Korea. Morphological characterization of the nanostructures was carried using a field-emission scanning electron microscopy (FE-SEM, Nova NanoSEM 230 FEI operating at 5kV, no metal coating was applied to the samples), transmission electron microscopy (JEM- 3011HR microscope operating at 80 kV), structural analysis by Raman spectra (LabRAM HR UV/vis/NIR Horiba Jobin-Yvon, France) and chemical analysis by X-ray photoelectron spectroscopy (Sigma Probe Thermo VG spectrometer using Mg Kα X-ray sources). The XPS spectra were curve fitted with a mixed Gaussian-Lorentzian shape using the freeware XPSPEAK version 4.1. Surface area and porosity were measured by Nitrogen adsorption and desorption isotherms at 77K using a BEL Japan Inc. Belsorp Mini II Surface Area and Pore Size Analysis system. Thermal gravimetric analysis was carried out in TA Instruments Q600 SDT thermal analyzer with a sample size of approximately 10 mg from 25 to 800 °C at a heating rate of 10 °C min^{-1} in air.

Electrochemical tests were conducted using CR2032 coin-type test cells assembled in argon-filled glove box. The working electrodes were composed of 0.5 mg of active material and a lithium foil separated by a micro-porous Celgard 2400 membrane. 1 M $LiPF_6$ dissolved in a 1:1 weight ratio of dimethyl and diethyl carbonates was used as the electrolyte solution. Galvanostatic charge-discharge cycling tests were performed using an WBCS 3000, Won-A-Tech, Korea battery testing system in the voltage range between 0.005 - 3 V.

***In-situ* synthesis of graphene-CNT hybrids**

A single step procedure was employed to synthesize carbon nano tubes anchored on graphene 3D nano-structures. Graphene oxide synthesized by modified Hummer's method, cobalt acetate and hydroquinone were mixed in a mortar-pestle in weight ratio of ratio of 1: 0.3 : 3. This mixture was transferred to a glass tube, partially sealed with a lid and subjected to microwave irradiation 700W for 150 seconds to form a fluffy powdery solid. The obtained product was washed with ethanol to remove any unreacted hydroquinone and subsequently dried in an oven at 100^0C for 60 minutes. [***Caution***: Large reactant volumes and subjecting the reactant mixture to prolonged microwave radiation causes explosions. This microwave reaction releases large amounts of gases and must be carried out in well ventilated room, preferably in a fume hood.]

Results and Discussion

The morphology and microstructure of the product studied by SEM (Figures 1(a) and (b)) shows dense carbon nanotube forests with typical lengths in the range of several micrometers to several tens of micrometers vertically anchored on porous graphene substrate. Corresponding TEM micrograph at low magnification shown in Figure 1(c) also confirms micrometer long carbon nanotubes with the cobalt catalyst particles at the head of nanotubes protruding out of graphene substrate. TEM micrographs at higher magnifications (Figures 1(c) and (d)) show curved CNTs with open ends. Additionally, most of the cobalt nano particle catalysts are either enclosed in carbon nanotubes or anchored on the surface of the graphene substrate. The mechanism of reduction of graphene oxide and subsequent formation of carbon nanotube can be explained in two concurrent steps. In the first step, the cobalt acetate under

microwave irradiation thermally decomposes to cobalt nano-particles which are anchored onto the intrinsic defects on graphene oxide surface caused by localized oxidation and/or mechano-chemical defects generated from sonication during the exfoliation process. Secondly, hydroquinone is oxidized to p-benzoquinone due to thermal decomposition and also by the catalytic activity of cobalt nano particles anchored on the graphene substrates. [45] With further increase in microwave radiation, the benzoquinone moieties are vaporized and are captured by the cobalt nano-particles which act as catalytic centers for aromatization process, involving both alkylation and dehydrogenation, leading to the formation of multi-walled carbon nanotubes. The growth of carbon nanotubes proceeds until the cobalt nano-particles lose their catalytic activity and are oxidized to cobalt oxide. Our newly discovered hydroquinone as CNT source is not only repeatable(Figure S1 in ESI file) but also can be extended to other catalysts like nickel and palladium (Figures S2 and S3 in ESI file).Furthermore, carrying out the experiment in absence of hydroquinone there is intense 'metal mediated etching'of graphene resulting in trenches and destruction of graphene substrate (Figure S4 in ESI file).

<<<<< Figure 1 >>>>>

The changes in chemical composition of GO, hydroquinone reduced graphene(HRG) and G-Co@CNT was investigated by X-ray photoelectron spectroscopy (XPS). Figure 2(a) shows the survey scans of the three materials in the range of 0 to 900 eV. Only C 1s and O 1s peaks are observed in GO, whereas the plot of HRG is feature less with only C1s being the discernible peak. In case of G-Co@CNT, in addition to C 1s and O 1s peaks, there is a Co 2p peak in the range of 770 to 810 eV with additional humps associated with Co 3s and Co 3p at 85-120 and 50-75 eV, respectively. The ratio of carbon to oxygen moieties, the C/O ratio is an important parameter to quantify the purity of graphene. From the plots shown in Figure 2(a) it is evident that there is spectacular increase in C/O ratio from 2.68 in graphene oxide to 8.87 and 8.52 in HRG and G-Co@CNT. The deconvoluted C1s and O1s XPS spectra are shown in Figure 2(b). The peak ~ 284.4 eV corresponds to C=C sp_2 bonded graphitic structure, whereas the peak at 285.1 eV is attributed to both defects in structure arising due to oxidation and also to carbonyl groups(C-O). The two peaks corresponding to carboxyl(C=O) and carboxylate

(O=C-OH) groups at 286.7 and 287.5 eV respectively corresponding to the well-known Lerf–Klinowski model of graphene oxide. [46] These observations are also reflected in the corresponding deconvoluted O1s spectra which show three peaks at 531.1-531.3 eV, 532.5 - 532.9 eV and the minor peak at 533.6 – 533.9 eV attributed to carbonyl groups, oxygen moieties in the form of carboxylic and hydroxyl groups and ether-type oxygen linkages, respectively.

There is a marked difference in the shape of deconvoluted C_{1s} XPS spectra of G-Co@CNT which is plotted in Figure 2(c) and is dominated by the predominant peak at 284.5 eV attributed to the C-C and C=C and the minor peaks at 286.2 and 288.3 eV attributed to remnant oxygen moieties existing as epoxy and carboxylic groups. The O_{1s} peaks in Figure 2(c) could only be fitted into one peak at binding energy of 532.2 eV corresponding to the chemisorbed oxygen belonging to defect. However, it must be said that this peak can also be attributed to chemisorbed moisture. [47] XPS spectroscopy is powerful tool to study the composition and structure of cobalt moieties, since it is very sensitive to ionic state of iron ex: Co^{2+} and Co^{3+} cations existing as cobalt monoxide, CoO and cobalt oxide, Co_3O_4, respectively. XPS spectra of Co 2p binding energy region plotted in Figure 2(d) show two distinct peaks at 780.5 and 795.9 eV indicating that the cobalt moieties exist in Co^{2+} state in the form of CoO . Of these two, the peak of Co $2p_{3/2}$ is dominant and stronger than Co $2p_{1/2}$ and the area of Co $2p_{3/2}$ peak is greater than that of Co $2p_{1/2}$ due to in spin–orbit (j–j) splitting. A clearly distinguishable peak observed at 787.1 eV is the satellite peak associated with Co $2p_{3/2}$, in addition to the small weakly discernible satellite hump at 803.1 eV which is the satellite peak for Co $2p_{1/2}$.

<<<<< Figure 2 >>>>>

The pioneering work by Tarascon group[48] on the utility of metal oxide nano-structures as anode materials for lithium ion batteries(LIB), have spurred intense focus on oxides of iron triad (Fe, Co and Ni). The theoretical lithium ion capacity of cobalt oxide is ~950mAhg^{-1} and due to its low cost and with ever increasing production since the start of this century[49], cobalt can be considered as a promising anode material. However, the two main problems associated with using cobalt oxides in LIB is its low intrinsic conductivity and progressive accelerated decrease in specific capacity during multiple

cycles. A natural way of overcoming these problems is by embedding cobalt oxide nano particles in mesoporous conductive substrates which offers advantages such as larger interfacial surface area, reduced ion diffusion length between the electrolyte and electrode, and the our newly developed 3D carbonaceous substrate provides a well inter-connected conductive network for efficient lithium ion transport.

<<<<<< Figure 3 >>>>>>

Galvanostatic cycling was carried out in the voltage range, 0.005−3.0 V, and at current rate of 250 mA g^{-1}. Figure 3(a) shows the voltage vs capacity plots of first three cycles of our three dimensional mesoporous G-Co@CNT electrodes. In the first cycle of a cathodic processing, exhibits a sharp peak at around 0.65 V, which remains almost constant in subsequent cycles, though at reduced intensity which can be attributed to the reduction of $Co^{2+} \rightarrow Co^{0}$ (lithium insertion) and the reaction of di-valent cobalt cations with the electrolyte solution.[18]

$$2CoO + 6Li^{+} + 6e^{-} \leftrightarrow Li_xCo_2O_3 \leftrightarrow 2Co + 3Li_2O$$

A broad anodic peak was observed at the potential of 1.36 eV corresponding to the oxidation of Co^0 to Co^2(lithium extraction). In the subsequent cycles, there was no significant change in the position of anodic peak albeit with reduced peak intensity, indicating that the electrochemical reaction proceeds in a repeatable fashion in the subsequent cycles. In the anodic cycle, a small hump at 2.01 V can also observed resulting from change in cobalt oxide oxidation states, i.e., $Co^{2+} \rightarrow Co^{3+}$.

Figure 3(b) shows the initial discharge (lithium insertion) and charge (lithium extraction) voltage profiles G-Co@CNT anodes exhibiting exceptional initial discharge and charge capacity of 2532.8 and 1270.4 mAh g^{-1}, respectively. The initial Coulombic efficiency of 48% can be calculated which is primarily due to the irreversible capacity loss occurring in the formation of solid electrolyte interface (SEI). The cycling profile during first discharge showed two distinct sloping plateaus, the first occurring in the region at ~1.5V, and the subsequent second plateau(~0.8V onwards) attributed to the Li^+ insertion into CoO anode and the formation of SEI film causing local disordering and solid-state. In the second

discharge curve, the flat plateau is replaced with a sloping curve originating at ~1.2 V due to the heterogeneous reaction mechanism of Li^+ insertion and extraction, and a discharge capacity of 1187 mAh g^{-1} is maintained. The irreversible capacity loss is associated with the formation of the SEI in the first cycle and the trapping of Li-ions at some locations of electrode materials. The morphology of our G-Co@CNT mesoporous nanostructures as observed by SEM shows carbon nanotubes anchored on graphene substrate wherein the lithium ions can be adsorbed on its surface; along the walls of carbon nanotubes, in the interstitial gaps between the nanotubes through the formation of Li_2C_6.[50] Consequently anodes based on our G-Co@CNT show very high discharge capacity of 1016 mAh g^{-1} even after 140 cycles is observed(Figure 3(c)). This high value of lithium ion capacity can be attributed to the synergetic effects of the following factors: lithium insertion in cobalt oxide (20.67 wt% as measured by TGA (Fig. S4 in associated Supplementary file); adsorption of Li ions on the surface of graphene and carbon nano-tubes; and also in between the mesopores of nanotubes. Comparing the lithium ion retention capacity of our 3D G-Co@NCNT composites with 2D cobalt decorated graphene (synthesized by our previously reported Doughnut method[51]), there is an almost 250% increase in capacity retention throughout the ~140 cycles indicating that presence of CNTs not only prevent the re-stacking of graphene, but also circumvent the aggregation of cobalt nano particles on cycling. Additionally the large surface area arising from mesoporosity, creates sufficient active surface area along the walls of nanotubes through which lithium ions can diffuse and adhere to the inter-wall spaces.

This high value of capacity retention even after prolonged cycling can be attributed to mesoporosity observed in SEM and measured by N_2-adsorption isotherms(Figure 3(d)). The existence of out of plane nano-pores of open ended carbon nanotubes combined with the micro-pores between the nanotube ensembles provide a short ion-transport pathway with minimal resistance and can accommodate the large volume changes of electrode material during lithiation/delithiation process. The N_2-adsorption isotherm of the G-Co@CNT exhibited a typical combined characteristics of type I/II, with a surface area of 612 m^2 g^{-1} and a total pore volume of 0.46 cm^3 g^{-1}. The sharp rise and hysteresis

loop in the P/P_0 range of ≈0.51–0.97 indicates the presence of micro/nano pores attributed to the 'spacer' functionality of nano-tubes which inhibits the restacking of graphene due to van der Waals attraction.

<<<<<< Figure 4 >>>>>>>>

Recently, post-mortem analysis of electrode materials after repeated cycles is being carried to study the lithium insertion mechanism,[52] effect of electrolytes[53] etc. We carried out post-mortem structural analysis of 3-D G-Co@CNT electrode after 140 cycles by SEM and a representative micrograph is shown in Figure 4. From the image, it can be observed that extensive lithium insertion not only occurred on graphene sheets but also on the carbon nanotubes so much so that the structure of nanotubes have transformed to lithium decorated CNT. Furthermore, the vertically standing CNT proves that our newly developed electrode is capable of withstanding the mechanical stresses occurring due to mixing and pressing during electrode preparation.

Conclusions

In conclusion, we have developed a fast and facile microwave method to effectively reduce and grow carbon nano tube spacers on graphene oxide by a single precursor, hydroquinone. Morphological studies by SEM and TEM showed a 3D mesoporous nano-architectures of nano-meter thin, micrometer long carbon nanotubes vertically anchored graphene substrate with surface areas to the tune of 612 $m^2 g^{-1}$ as tested by nitrogen adsorption/desorption studies. When applied as anode in lithium ion batteries, the synthesized nanostructure exhibited exceptionally high lithium storage capacity of 1016 $mAhg^{-1}$ even after prolonged cycling emphasizing the strong synergy between the graphene substrate and carbon nanotubes.

ACKNOWLEDGMENT. This work was supported by National Research Foundation of Korea(NRF) grant of the Korea government(MSIP) through GCRC-SOP(No. 2011-0030013).

REFERENCES

[1] K. S. Novoselov, A. K. Geim, S. V. Morozov, D. Jiang, Y. Zhang, S. V. Dubonos, I. V. Grigorieva and A. A. Firsov, *Science* 2004, **306**, 666.

[2] S. Stankovich, D. A. Dikin, R. D. Piner, K. A. Kohlhaas, A. Kleinhammes, Y. Jia, Y. Wu, S. T. Nguyen and R. S. Ruoff, *Carbon* 2007, **45**,1558.

[3] C. Gomez-Navarro, J. C. Meyer, R. S. Sundaram, A. Chuvilin, S. Kurasch, M. Burghard, M. Burghard, K. Kern and U. Kaiser, *Nano Lett.* 2010, **10**, 1144.

[4] H. Guo, M. Peng, Z. Zhu and L. Sun, *Nanoscale* 2013, **5**, 9040.

[5] G. Williams, B. Seger and P. V. Kamat, *ACS Nano 2008*, **2**, 1487.

[6] S. S. J. Aravind, V. Eswaraiah and S. Ramaprabhu, *J Mater Chem. 2011*, **21**,17094.

[7] S. Pei, and H. M. Cheng, *Carbon 2012*, **50**, 3210.

[8] W. Chen and L. Yan, *Nanoscale*, *2011*, **8**, 3132.

[9] R. S. Edwards and K. S. Coleman, *Nanoscale*, *2013*, **5**, 38.

[10] H. L. Poh, F. Sanek, A. Ambrosi, G. Zhao, Z. Sofer, and M. Pumera, *Nanoscale*, *2012*, **4**, 3515.

[11] J. R. Lomeda, C. D. Doyle, D. V. Kosynkin, W. F. Hwang, J. M. Tour, *J. Am. Chem. Soc. 2008*, **130**, 16201.

[12] M. Lotya, Y. Hernandez, P. J. King, R. J. Smith, V. Nicolosi, L. S. Karlsson, F. M. Blighe, S. De, Z. Wang, I. T. McGovern, G. S. Duesberg, and J. N. Coleman, *J. Am. Chem. Soc. 2009*, **131**, 3611.

[13] J. Xu, K. Wang, S. Z. Zu, B. H. Han, Z. Wei, *ACS Nano 2010*, **4**, 5019.

[14] H. Sun, X. Sun, T. Hu, M. Yu, F. Lu, and J. Lian, *J. Phys. Chem. C* **2014**, *118*, 2263.

[15] V. Sridhar, I. Lee, Y. S. Yoon, H. H. Chun, H. Park, *Carbon 2013*, **61**, 633.

[16] F. Zheng, M. He, Y. Yang, and Q. Chen, *Nanoscale*, *2015*, **7**, 3410.

[17] G. Compagnini, M. Sinatra, P. Russo, G. C. Messina, O. Puglisi, and S. Scalese, *Carbon*, *2012*, **50**, 2362.

[18] M. Zhi, C. Xiang, J. Li, M. Li, and N. Wu, *Nanoscale*, *2013*, **5**, 72.

[19] W. Sun and Y. Wang, *Nanoscale*, *2014*, **6**, 11528.

[20] L. Fu, K. Tang, K. Song, P. A. van Aken, Y. Yu, and J. Maier, *Nanoscale*, *2014*, **6**, 1384.

[21] V. C. Tung, L.-M. Chen, M. J. Allen, J. K. Wassei, K. Nelson, R. B. Kaner, and Y. Yang, *Nano Lett. 2009*, **9**, 1949.

[22] C. Zhu and S. Dong, *Nanoscale*, *2013*, **5**, 1753.

[23] D. H. Youn, S. Han, J. Y. Kim, J. Y. Kim, H. Park, S. H. Choi, and J. S. Lee. *ACS Nano 2014*, **8**, 5164.

[24] S. Biswas, and L. T. Drzal, *Chem. Mater. 2010*, **22**, 5667.

[25] J. W. Lee, A. S. Hall, J. D. Kim, T. E. Mallouk, *Chem. Mater. 2012*, **24**, 1158.

[26] Y. Zhu, L. Li, C. Zhang, G. Casillas, Z. Sun, Z. Yan G. Ruan, Z. Peng, A.-R. O. Raji, C. Kittrell, R. H. Hauge, and J. M. Tour, *Nat. Comm. 2012*, **27**,1225.

[27] B. P. Vinayan, R. Nagar, V. Raman, N. Rajalakshmi, K. S. Dhathathreyan, and S. Ramaprabhu, *J. Mater. Chem.*, *2012*, **22**, 9949.

[28] D. D. Nguyen, N.-H. Tai, S.-Y. Chen, and Y.-L. Chueh, *Nanoscale*, *2012*, **4**, 632.

[29] L. L. Zhang, Z. Xiong and X. S. Zhao, *ACS Nano 2010*, **4**, 7030.

[30] S.H. Lee, V. Sridhar, J.H. Jung, K. Karthikeyan, Y.S. Lee, R. Mukherjee, N. Koratkar, and I.K. Oh, *ACS Nano*, *2013*, **7**, 4242.

[31] M. Liu, Y.-E. Miao, C. Zhang, W. W. Tjiu, Z. Yang, H. Peng, and T. Liu, *Nanoscale*, *2013*, **5**, 7312.

[32] K. P. Prasad, Y. Chen and P. Chen, *ACS Appl. Mater. Inter. 2014*, **6**, 3387.

[33] S. Mao, G. Lu, and J. Chen, *Nanoscale*, *2015*, **7**, 6924.

[34] C. Wu, X. Huang, X. Wu, L. Xie, K. Yang, and P. Jiang, *Nanoscale*, *2013*, **5**, 3847.

[35] Y. K. Kim and D. H. Min. *Langmuir 2009*, **25**, 11302.

[36] K. Kumar, Y.-S. Kim, X. Li, J. Ding, F. T. Fisher, and E.-H. Yang, *Chem. Mater. 2013*, **25**, 3874.

[37] S. Chen, P. Chen, and Y. Wang, *Nanoscale*, *2011*, **3**, 4323.

[38] X. Zhu, G. Ning, Z. Fan, J. Gao, C. Xu, W. Qian, and F. Wei, *Carbon*, *2012,* **50**, 2764.

[39] X. Dong, Y. Ma, G. Zhu, Y. Huang, J. Wang, M. B. Chan-Park, L. Wang, W. Huang, and P. Chen, *J. Mater. Chem.*, **2012**, *22*, 17044.

[40] V. Sridhar, H. J. Kim, J. H. Jung, C. Lee, S. Park, and I. K. Oh, *ACS Nano*, **2012**, *6*, 10562.

[41] Z. Liu, J. Wang, V. Kushvaha, S. Poyraz, H. Tippur, S. Park, M. Kim, Y. Liu, J. Bar, H. Chen, and X. Zhang, *Chem. Commun.*, **2011**, *47*, 9912.

[42] C. N. R. Rao and R. Sen. *Chem. Commun.*, **1998**, *15*, 1525.

[43] V. Sridhar, I. Lee, H. H. Chun, and H. Park, *Carbon*, **2015**, *87*, 186.

[44] G. Wang, J. Yang, J. Park, X. Gou, B. Wang, H. Liu, and J. Yao, *J. Phys. Chem. C* **2008**, *112*, 8192.

[45] R. J. Radel, J. M. Sullivan and J. D. Hatfield, J.D. *Ind. Eng. Chem. Prod. RD* **1982**,*4*, 566.

[46] K. P. Loh, Q. Bao, G. Eda, M. Chhowalla, *Nat. Chem.* **2010**, *2*, 1015.

[47] C. Sun, and J. C. Berg, *Adv. Coll. Interf. Sci.* **2003**, *105*,151.

[48] P. Poizot, S. Laruelle, S. Grugeon, L. Dupont, J. M. Tarascon *Nature* **2000**, *407*, 496.

[49] http://en.wikipedia.org/wiki/Cobalt

[50] F. Disma, L. Aymard, L. Dupont, J. M. Tarascon. *J. Electrochem. Soc.* **1996**, *143*, 3959.

[51] S. Vadahanambi, J.H. Jung, I.K. Oh. *Carbon*, **2011**, *49*, 4449.

[52] H. Buqa, A. Wursig, D. Goers, L. J. Hardwick, M. Holzapfel, P. Novak, F. Krumeich, M. E. Spahr. *J. Power Sources*, **2005**, *146*, 134.

[53] M. Holzapfel, C. Jost, A. Prodi-Schwab, F. Krumeich, A. Würsig, H. Buqa, P. Novak. *Carbon*, **2005**, *43*, 1488.

Graphical abstract.

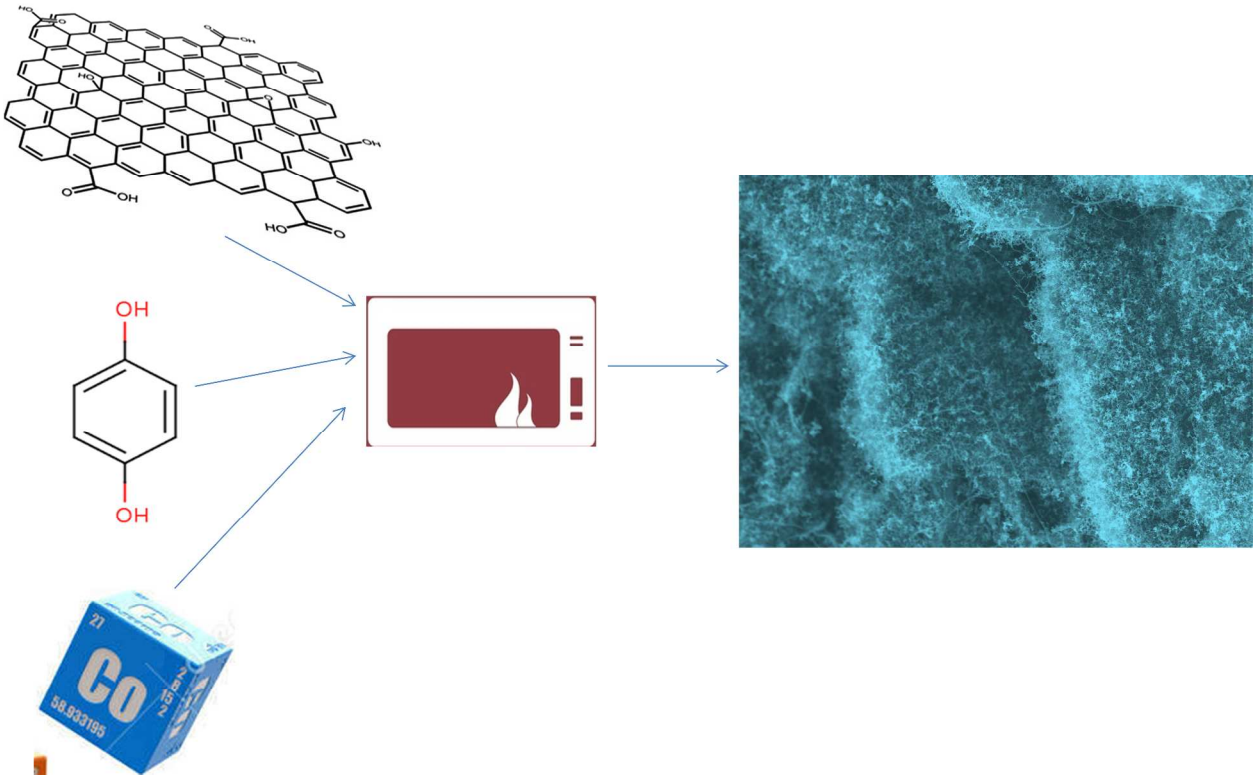

In this study, we report a one-step, all solid-state microwave procedure for simultaneous reduction and concurrent growth of carbon nanotubes on graphene from a single precursor, namely hydroquinone.

Captions to figures

Figure 1 SEM(a and b) and TEM(c and d) micrographs of nitrogen doped carbon nanotubes vertically anchored on graphene substrate at low and high magnification. Scale bars are 5 μm, 2 μm, 500 nm and 200 nm in (a), (b), (c) and (d) respectively.

Figure 2 XPS survey scan (a); Deconvoluted C1 s and O1 s spectra of graphene oxide(b) and G-Co@CNT (c) and deconvoluted Co 2p spectra(d).

Figure 3 Cyclic voltammetry studies(a), Galvanostatic discharge−charge cycling curves(b), charge-discharge capacity vs number of cycles(c) and BET surface area of G-Co@CNT. Insert in Figure (d) is pore size distribution.

Figure 4 Post-mortem representative SEM micrograph of 3D G-Co@CNT anode after 140 cycles.

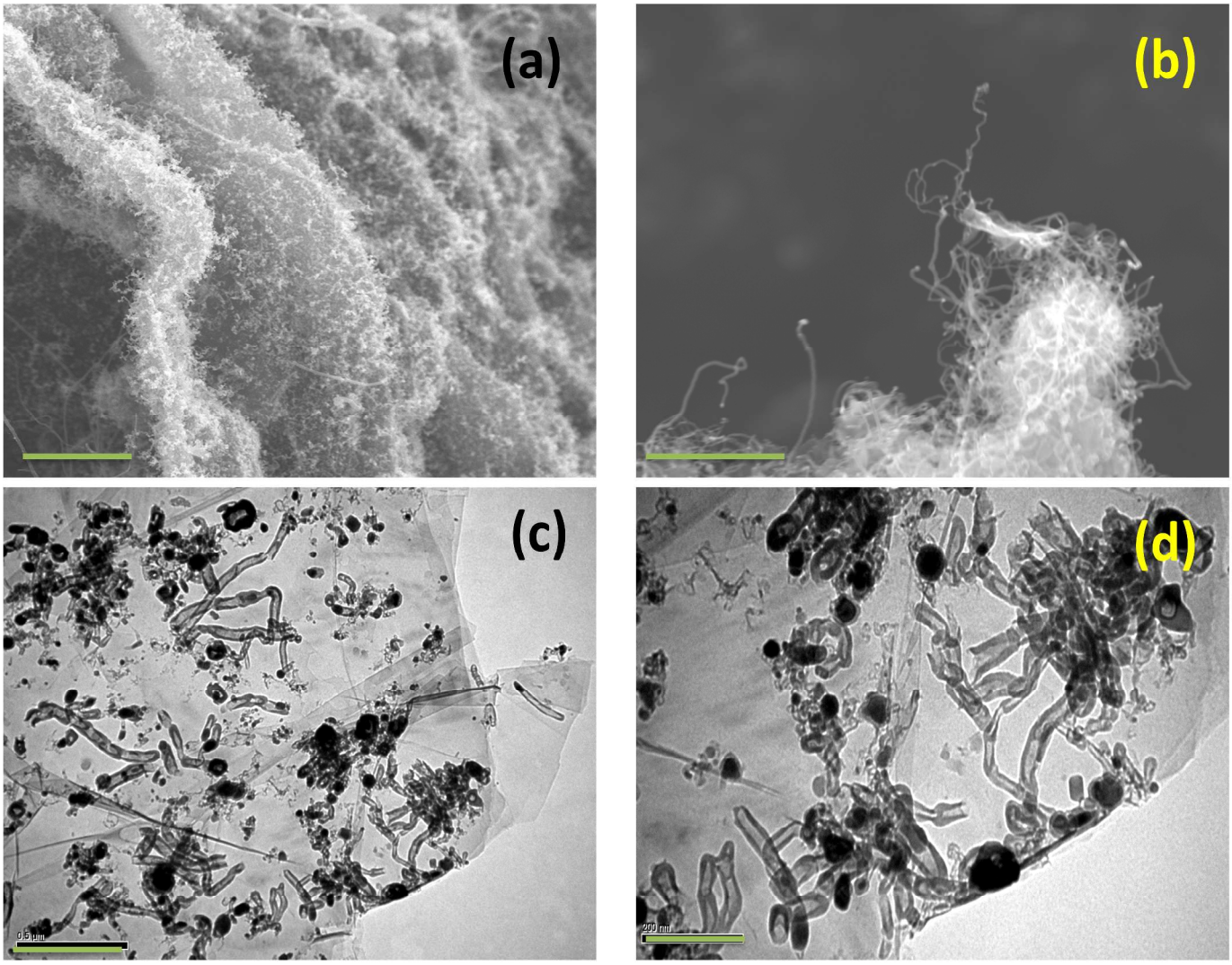

Figure 1

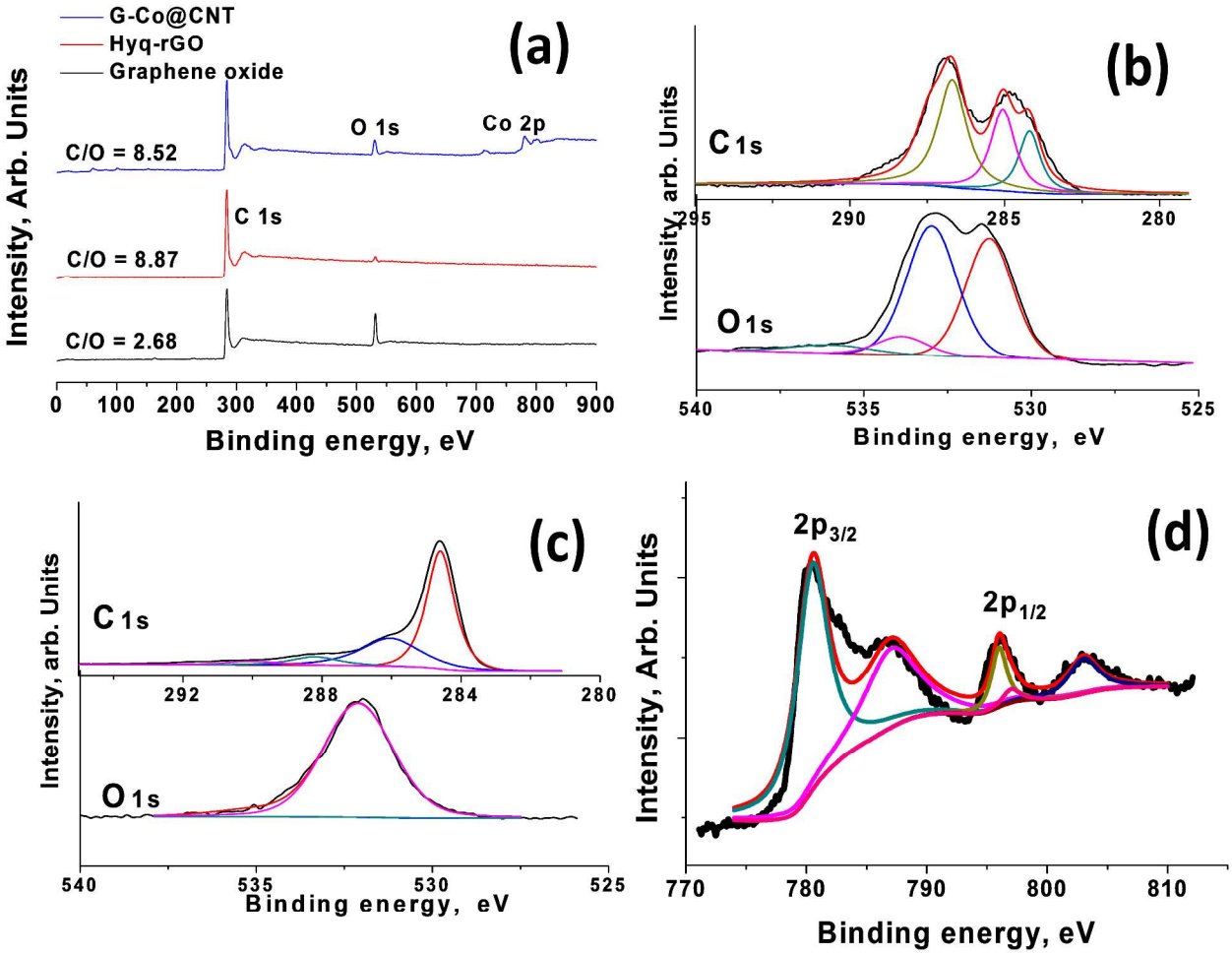

Figure 2

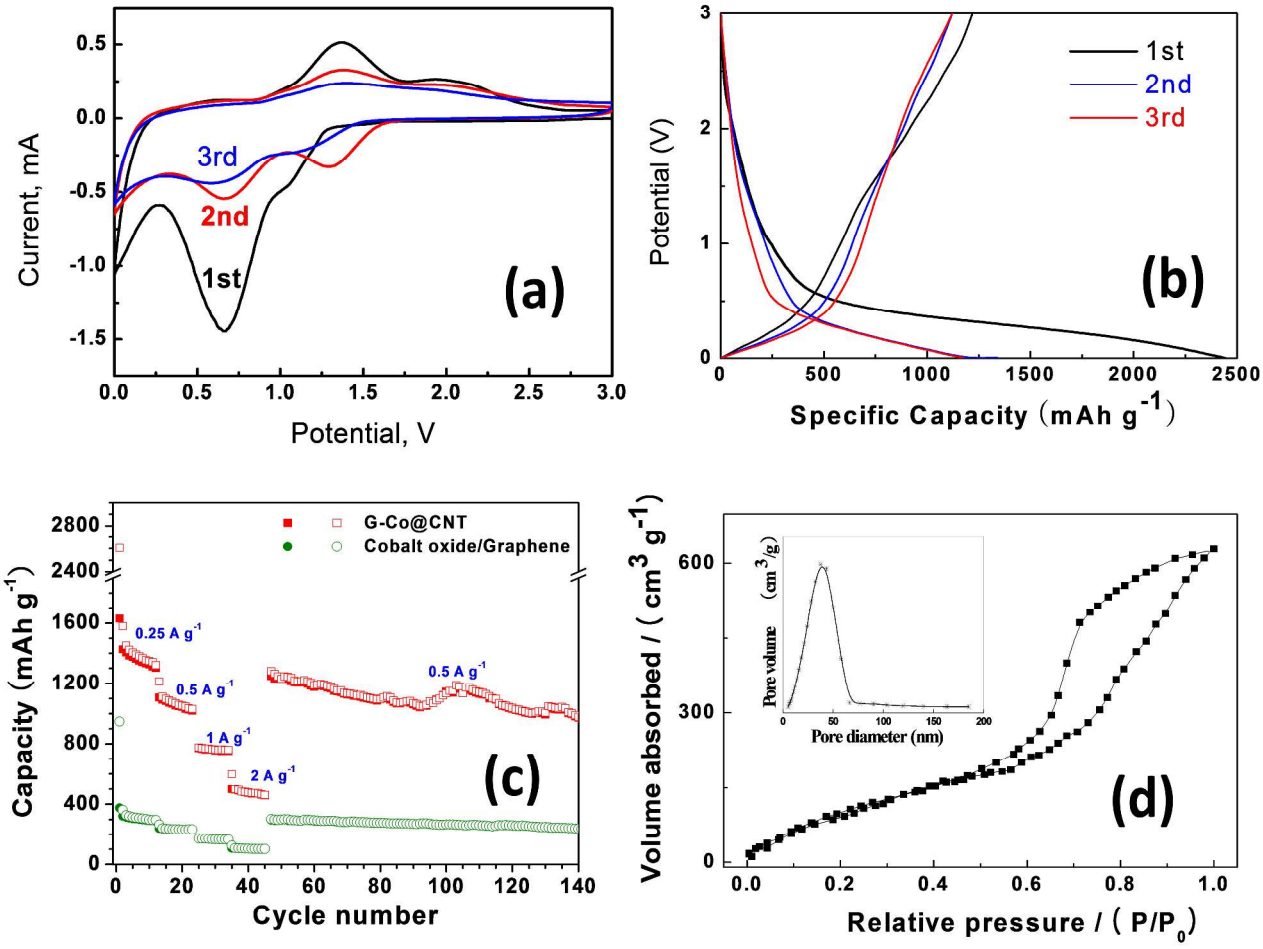

Figure 3

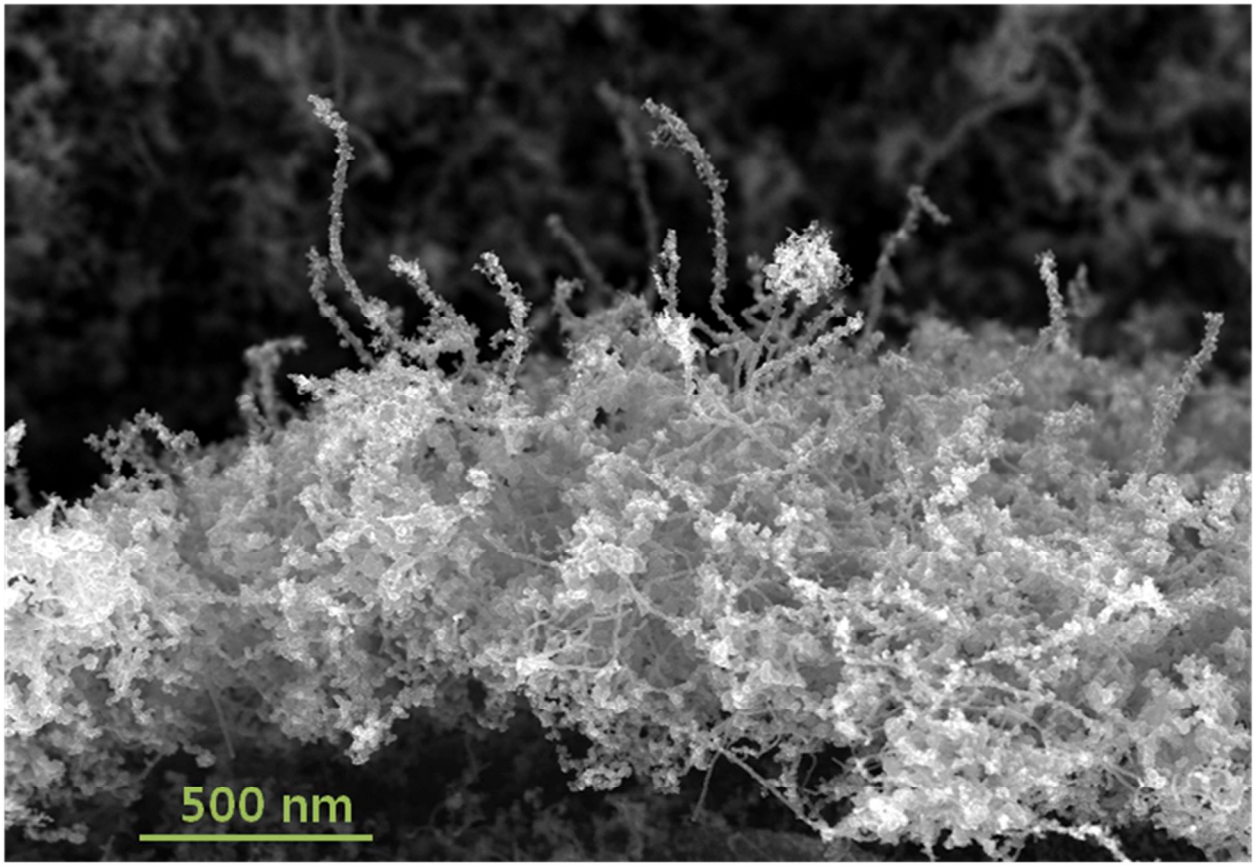

Figure 4